Optimization of the Geometry of a Thermoelectric Combustion Chamber for Micropower Production

Thesis

Presented in Partial Fulfillment of the Requirements for the Honors Research Distinction in Mechanical Engineering in the Undergraduate School of The Ohio State University

By

Mark Verosky

Undergraduate Program in Mechanical Engineering

The Ohio State University

2018

Defense Committee

Joseph Heremans, Advisor

Sandip Mazumder

Abstract

Common modes of power production require the use of dynamic devices that are heavy and require a considerable amount of maintenance. Thermoelectric materials generate electricity using a physical phenomenon known as the Seebeck effect. The Seebeck effect produces a voltage difference from the temperature gradient in a material. Therefore, by heating up one end of a material and keeping the other end at a lower temperature, a voltage difference is produced. The objective of this research was to create a portable means of power production from readily available thermoelectric materials and determine ways in which the geometry of this device could be modified to improve the TEG's overall performance. Construction of the device consisted of three main components: a small camping stove, butane fuel canister, and a thermopile constructed of type E (Nickel-Chromium / Constantan) thermocouples. The thermopile also acted like a flashback arrestor, preventing the flame from propagating back to the propane/butane fuel canister. During testing, the fuel exited the canister, flowed through the thermopile and then ignited. Changing the geometry of the design of the combustion chamber were analyzed to determine which designs improved the performance of the TEG.

Acknowledgments

Without the help of both Professor Heremans and Michael Adams, the completion of this study would not have been possible. Their support throughout this project has been of a tremendous help.

Additionally, I would like to thank Professor Sandip Mazumder.

Table of Contents

List of Tables

List of Figures

List of Symbols

A_{jet}	Area of the Jet, Cross-Sectional to the Flow
c_p	Specific Heat
F	Flow Function
H	Distance Between Top of Thermopile and Top of Main Tube
I	Electrical Current
k	Thermal Conductivity
L	Length
$\dot{m}$	Mass Flow Rate
N_{tc}	Number of Thermocouples in a Thermopile
P	Power
P^*	Critical Pressure
P_0	Vapor Pressure
R	Electrical Resistance
T	Temperature
T_0	Critical Temperature
T_c	Cold Side Temperature
T_h	Hot Side Temperature
T_{Room}	Room Temperature
V	Voltage
V_{out}	Output Voltage
V_{tc}	Thermocouple Voltage
$V_{tc,ave}$	Average Thermocouple Voltage
ZT	Figure of Merit
ZT_{ave}	Average Figure of Merit
α	Seebeck Coefficient
α_A	Seebeck Coefficient of Material A
α_B	Seebeck Coefficient of Material B
α_{AB}	Relative Seebeck Coefficient
γ	Specific Heat Ratio
ζ	Fuel Efficiency Coefficient
$\eta_{p,max}$	Max Thermoelectric Generator Efficiency
ρ	Electrical Resistivity
σ	Electrical Conductivity

Chapter 1. Introduction

1.1 Background

Much research has been done on thermoelectric generators (TEGs) as a means of waste heat recovery. This research is focused around increasing the efficiency of the overall system by utilizing a TEG to generate electricity from the system's waste heat. Considerable attention has been allotted towards this subject due to the increase in material figure of merits[1] at temperatures seen in the exhaust system of internal combustion engines (ICEs) in consumer vehicles (Rowe, 2006). Figure 1 shows the figure of merit of various materials in the temperature range consistent with consumer automobile exhaust temperatures (Chen & Zheng, 2011)d. The higher the figure of merit, the more efficient a TEG is at converting waste heat into useable electrical power.

While materials with high figures of merit exist, they are often difficult to produce consistently and in bulk. This difficultly to consistently produce these materials results in a high price point that makes their application in industry unlikely or even impossible. Therefore, industrial thermoelectric materials are limited to materials that can be

[1] Figure of Merit: A dimensionless parameter, derived from material properties, that is used to gauge the performance of thermoelectric materials. The larger the figure of merit is, the better the thermoelectric performance of the material.

$$ZT = \frac{\sigma\alpha^2 T}{k} = \frac{\alpha^2 T}{\rho k} \quad (1)$$

produced in bulk and thus lower figures of merit. Industrial thermoelectric materials typically have figures of merit of 1 or less.

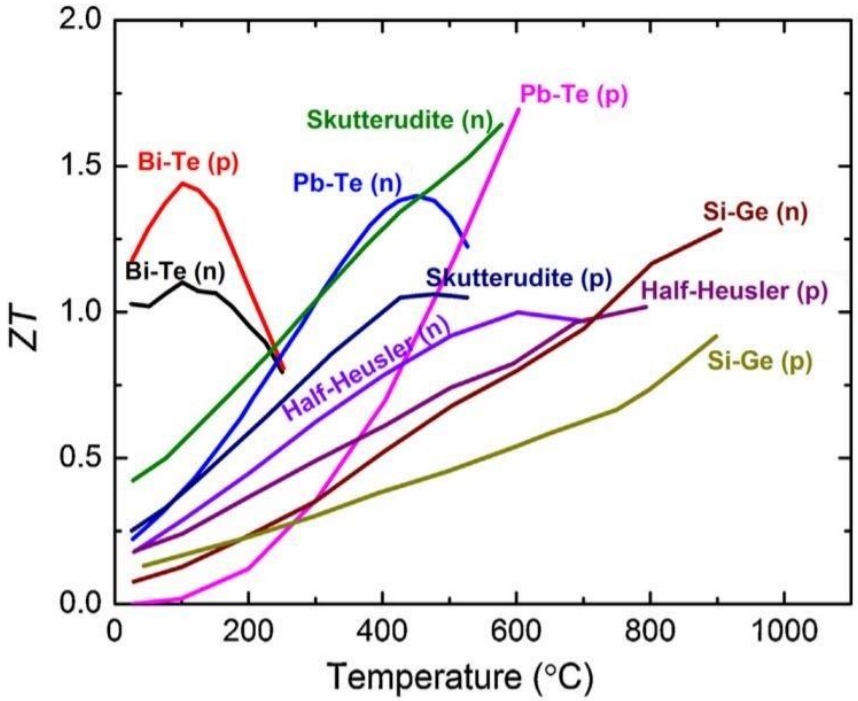

Figure 1: Figure of Merit vs Temperatures of Materials (Chen & Ren, 2013)

1.2 Micro Power Generation with Thermoelectric Materials

Using thermoelectrics for micro power generation has practical applications in areas that have unreliable or no electrical grid. Many of these locations are not easily accessible and thus creates difficultly in bringing large form generators. Generating a reliable and easily transportable generator that can provide power for an individual at a low cost could permit access to electricity on demand in more areas.

In addition to power generation for the individual in remote areas, the creation of a similar small-scale generator could prove advantageous to electrical equipment in

environments where commercial power is unavailable. In addition to the ease of getting equipment to remote locations, having a generator that requires little to no maintenance is also a quality that is sought after.

Previous research has been conducted on the applicability of thermoelectrics for the applications specified (Corry, Moreland, & Strickland, 1960), (Plevyak, 1967). Both studies used propane gas as their means to create the hot side temperature of their TEG. In one study the use of the thermoelectric generator was to power telephone microwave equipment in remote locations.

1.3 Reason for Study

A contemporary design of a thermoelectric generator could yield better efficiency than those found in previous studies by utilizing larger temperature gradients. The goal of this study was to utilize fossil fuels in a TEG and modify the geometry to see how the performance of the TEG is affected. Additionally, it was desired to create a TEG that was created with the use of bulk materials.

Previous research on the topic did not utilize the temperature gradients possible with fossil fuels. Additionally, the hot side temperature of the thermoelectric was limited to a maximum temperature of 620[^{o}C] due to the low melting temperatures of the materials used (Corry, Moreland, & Strickland, 1960). Thermoelectric materials that can withstand the flame temperature of fossil fuels, however, typically have lower figures of merit. This lower figure of merit results in a decrease in overall efficiency of the TEG.

Since TEGs are heat engines, their efficiency is dictated by the temperature differential. Therefore, creating a large temperature differential between the hot and cold sides of the TEG leads to an increase in efficiency for the TEG, regardless of the figure of merit. The correlation between figure of merit, TEG efficiency, and temperature differential is shown in Figure 2, with the efficiency being determined by equation 1. While creating a larger temperature differential does result in better efficiency, it should be noted that materials that can withstand higher temperatures yield figure of merit values lower than those found at lower temperatures.

$$\eta_{p,max} = \frac{T_h - T_c}{T_h}\left[\frac{\sqrt{1 + ZT_{ave}} - 1}{\sqrt{1 + ZT_{ave}} + \frac{T_c}{T_h}}\right] \quad (1)$$

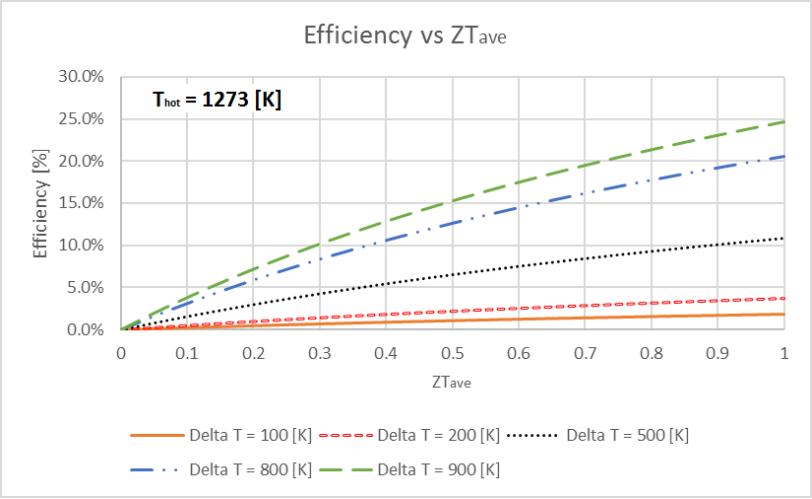

Figure 2: Efficiency vs Average Figure of Merit

Thermoelectric materials have no moving parts and thus require very little maintenance. This characteristic is desirable in circumstances where the generator is operating in remote locations where maintenance operations are difficult. Additionally, combustible fuels contain anywhere from 10 to 100 times the energy density of current batteries. Therefore, fuel is more desirable to transport than batteries since it has the potential to produce more power output per unit mass (Snyder, 2008). For the TEG to match the same power density as a battery, however, it must obtain an efficiency of around 10% (Snyder, 2008).

The scale of a thermoelectric generator does not have a significant impact on its efficiency. Thermoelectric materials are easily scalable without a loss in efficiency. This is not the case with other forms of power production, in heat engines; the size of the engine has a considerable factor on efficiency.

Chapter 2: Thermoelectric Generator (TEG)

2.1 Seebeck Effect and Thermoelectric Materials

The physical phenomena behind TEGs is the Seebeck effect. The Seebeck effect was discovered by Thomas Johann Seebeck in 1821 and states that an electromotive force (emf) is produced when two dissimilar materials have junctions at two different temperatures (Britannica, 1998). In TEGs, these two dissimilar materials are a n-type material and a p-type material. A n-type material has a Seebeck coefficient[2] less than 0 ($\alpha < 0$), whereas a p-type material has a Seebeck coefficient greater than 0 ($\alpha > 0$). When the n-type and p-type materials are connected, a relative Seebeck coefficient between the two materials can be determined; this equation can be seen in equation 2. Units for the Seebeck coefficients of some materials at room temperature can be seen in Table 1.

$$\alpha_{AB} = \alpha_A - \alpha_B \tag{2}$$

[2] Seebeck Coefficient: Measure of a material's ability to induce a voltage in response to a temperature differential because of the Seebeck effect. Seebeck coefficients are typically given in μV/K, which represents the voltage difference between the two ends of the material per kelvin difference between the two ends.

Table 1: Seebeck Coefficient of Materials (Lasance, 2006)

Material	Seebeck Coefficient [μV/K]
Se	900
Te	500
Si	440
Ge	300
Antimony	47
Nichrome	25
Copper	6.5
Platinum	0
Nickel	-15
Constantan	-35
Bismuth	-72
PbTe	-180

In n-type materials, electrons are the carrier elements[3] and a negative potential is formed on the cold end of the material. P-type materials have holes[4] as their carrier elements and have a positive charge build up on the cold end of the material. Figure 3 illustrates how the charge carries build up in thermoelectric materials.

[3] Carrier Elements: particles which carry an electrical charge and are free to move.
[4] Holes: Missing electrons around an atom which creates a positive charge.

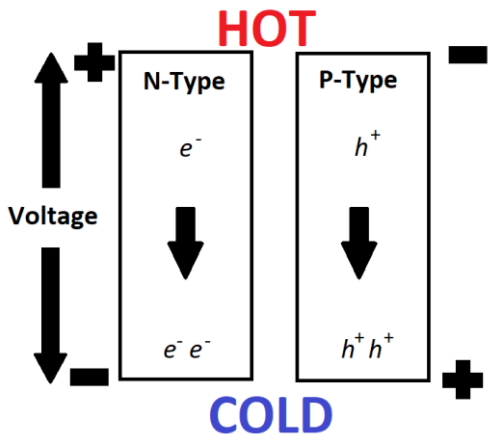

Figure 3: Thermoelectric Module (Wiegand, 2015)

2.2 Thermoelectric Generator

A thermoelectric generator is a solid-state device that creates electrical energy from a temperature gradient. These generators typically contain many thermocouple pairs in series so that the voltage generated by each thermocouple is added together. Many thermocouples in series is commonly known as a thermopile. Figure 4 demonstrates how these thermocouples would be connected in a thermoelectric generator.

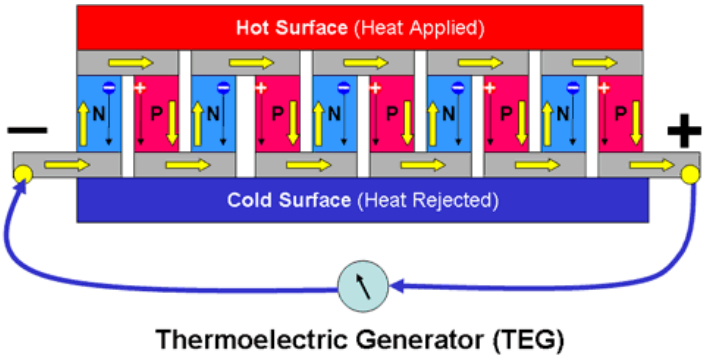

Figure 4: Thermoelectric Generator (TEG) Illustration (Design and Implementation of Thermoelectric Generator, n.d.)

Chapter 3: Methodology

3.1 Introduction

In this study, the goal was to look at readily available bulk materials and create a TEG that operates using fossil fuels. The geometry of the TEG was to be modified in several ways to determine how it affects the overall performance of the TEG.

3.2 Selection of Combustion Device and Fuel

When selecting the combustion device to be used, the first thing considered was the type of fuel being used and the cost and attainability of the fuel. Another point of concern was the ease of the combustion device to be modified or created. With these two parameters in mind a camping stove made by MSR® known as the PocketRocket® was used as the means to combust the fuel. Figure 5 shows a picture of the stove before any modifications were made as well as the nomenclature used when referring to the various parts of the Combustion Device.

3.2.1 Modification of MSR® PocketRocket®

After looking over the device, it was determined that the tube in which the fuel flowed up through could be filled with thermocouples. The bottom of the thermocouple[5] would be cooled due to forced convection via the fuel/air mixture moving upwards

[5] Bottom of Thermocouple: This will refer to the side of the thermocouple that is closest to the fuel canister (reference Figure 5)

towards the combustion chamber. The top of the thermocouples[6] would then poke out of the tube into the combustion chamber.

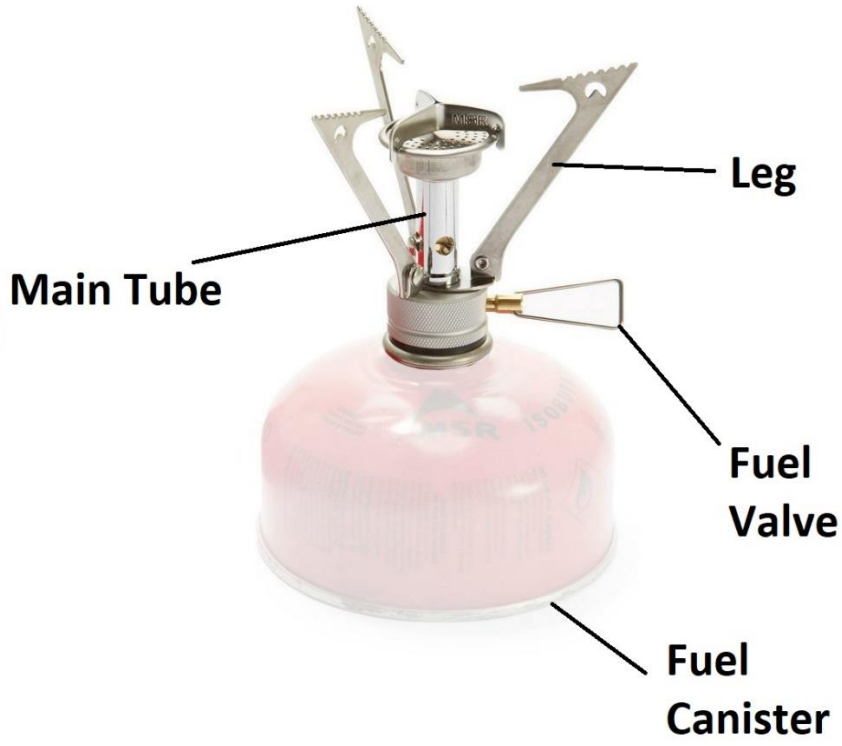

Figure 5: MSR® PocketRocket® (Amazon, n.d.)

For the thermocouples to stick out as previously described, the device at the end of the main tube was removed. Upon removal of this device and examination of the inside of the main tube, it was determined that when thermocouples were placed inside, there existed a potential of a short since the main tube is constructed of metal. To alleviate this concern, the inside of the main tube was coated with a layer of Boron

[6] Top of Thermocouple: This will refer to the side of the thermocouple that is closed to the combustion chamber. (reference Figure 5)

Nitride[7]. Care was taken to ensure that the jet[8] was protected and not covered in boron nitride spray. Figure 6 shows the combustion device with a boron nitride coating on the inside of the main tube.

Figure 6: Modified Combustion Device with Boron Nitride Coating

3.2.2 Selection of Fuel

As a camping stove, the PocketRocket® could connect to a standard fuel canister that had various fuels. The type of fuel that the team selected was made by STERNO, a picture of this fuel canister can be seen in Figure 23 in Appendix B. For the experiments ran in this project, Sterno Fuel was used. Since the exact composition of the Sterno[9] fuel

[7] Boron Nitride: Chemically inert material that has a high thermal electrical resistance and resistant to high temperatures (Accuratus, 2013).
[8] Jet: Hole in which the fuel exits the base of the combustion device and enters the main tube.
[9] Attempt to contact Sterno® and determine their fuel mixture was made. No reply was received as of the publishing of this document.

was not known, fuel mixtures of other fuels used for backpacking stoves were examined (MSR, 2018) (Katadyn Group, 2018). Based on the examination of these other backpacking fuels, it was concluded that the fuel was likely to contain a mixture of approximately 70% Butane and 30% Propane. Therefore, for all calculation this was the assumed gas mixture used for fuel. The relevant material properties associated with this gas mixture can be seen in Appendix A.

3.3 Selection of Thermoelectric Materials

When selecting the thermoelectric materials, it had to be ensured that the materials could first withstand the temperature of a propane/butane mix. Therefore, the flame temperature of different propane/butane mixtures were investigated. Adiabatic Flame temperatures of butane, propane, and a propane/butane mix is approximately 1970 [^{o}C][10] (Engineering ToolBox, 2003). The temperature attained in an adiabatic flame, however, is not what is obtained in practice. This is due to factors such as incomplete combustion and heat transfer (Adiabatic Flame Temperature, n.d.).

Based on a study done by Sharma (Sharma, Sheoran, & Shakher, 2012), the flame temperature of approximately 850 [^{o}C] was obtained with butane gas with a diffusion flame (Sharma, Sheoran, & Shakher, 2012). Higher temperatures were reached in the study conducted by Sharma but they were done so with premixed butane/air mixtures. Due to the ease of availability of simple propane/butane mixtures and the difficulty of modifying the PocketRocket® to make a premixed butane/air mixture, it was determined

[10] Adiabatic Flame Temperature in the presence of air at 20 [^{o}C] and at atmospheric pressure.

that the flame produced would be that of a diffusion flame. Therefore, a material selected for use in the TEG had to be able to withstand at least a temperature of approximately 1000 [^{o}C][11].

Many of the thermoelectric materials that had high figures of merit and could withstand temperatures of 1000 [^{o}C] required synthesis in the lab and were not readily available in bulk or were of substantial cost. As one of the primary goals associated with this project was to create a TEG that was low-cost. The use of high figure of merit materials synthesized in the lab that performed at the temperatures desired was cost prohibitive. Instead, thermocouples that could withstand temperatures of 1000 [^{o}C] or greater and their relative Seebeck Coefficients were examined.

Figure 6 shows a plot of different thermocouple types and their voltage output in relation to temperature gradient. It can be seen from this figure that the thermocouple that performed the best was a type-E and can withstand temperatures of 1000 [^{o}C] or greater.

[11] An increase from the 850 [^{o}C] flame temperature measured by Sharma's study to at least 1000 [^{o}C] was expected due to the flame being contained inside a chamber.

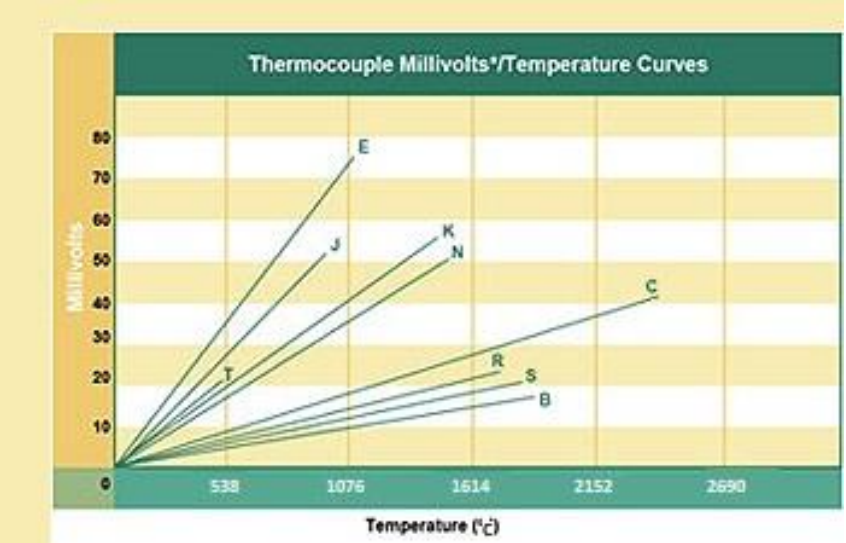

Figure 7: Thermocouple Millivolts vs Temperature Gradient [^{o}C] (Thermocouple info, n.d.)

3.4 Thermocouples and Construction of Thermopile

Type-E thermocouples consist of an n-type material, Constantan[12], and a p-type material, Nickel-Chromium[13]. The relevant Seebeck coefficient between the two materials is approximately 60 [μV/K] and remains relevantly constant through the temperatures between -250 to 900 [^{o}C] in oxidizing atmospheres (Thermocouple info, n.d.). Since type-E thermocouples had the highest Seebeck coefficient of all the thermocouples investigated, could withstand the temperatures, and was readily available, it was selected to be utilized in the TEG.

[12] Constantan: 55% Copper 45% Nickel.
[13] Nickel Chromium: Also known as Nichrome. 90/10 Nickel Chromium Alloyd

Upon determination that a type-E thermocouple was best suited for this study, two thermopiles capable of generating a maximum output voltage of 750 [mV] were ordered[14]. These thermopiles were then manipulated to create different thermopile geometries for experimentation.

3.4.1: Stock Thermopile

The thermopile that was ordered had a metal encasing guarding the thermoelectric materials. Therefore, to gain access to the materials underneath the metal covering, the metal encasing had to be removed. To remove this casing, a Dremel® tool with a reinforced cutoff wheel attached was used to cautiously grind down the metal encasing until it was gone.[15] After removing enough of the metal encasing it could be opened and the thermopile removed. Figure 8 shows the thermopile that was removed.

The geometry of the stock thermopile as well as other information regarding it can be seen in Appendix C.1

3.4.2: Thermopile B

Thermopile B[16] was created to decrease the overall the length of the thermopile. Reducing the length of the thermopile would result in a decrease in resistance which then results in an increase in power[17]. The relationship between the length of the thermopile and resistance is shown in equations 3.

---

[14] Figure 24 in Appendix B shows the bag that the thermopiles were delivered in.
[15] Figure 25 in Appendix B shows a picture of the Dremel® tool being used to grind down the metal encasing of the original thermopile.
[16] For more information regarding the methods used to create Thermopile B as well as its dimensions, please refer to Appendices C and D respectively.
[17] This is based on Ohm's Law: V=IR and its relationship with the equation P=IV. Using these two equations, the following expression is formed: $P = \frac{V^2}{R}$. Here it is clearly demonstrated that decreasing length of the thermopile could result in a decrease in R and hence an increase in power and efficiency.

$$R = \frac{\rho\, L}{A} \tag{3}$$

Figure 8: Stock Thermopile Next to Original Metal Encasing

3.5: Altering TEG Parameters

One of the primary goals of the study was to determine the changes geometry had on the performance of the TEG. There were 3 parameters that were altered in this study:

1. Length of Thermopile Legs
2. Position of Thermopile B's top relative to the top of the main tube
3. Addition of the Combustion Chamber and alteration of its design

Each of these tests were conducted using the same fuel in the same room using the same combustion device, a modified PocketRocket®. The Voltage of the thermopile was measured using a Keithley 2100 6 ½ DIGIT multimeter. A camera recorded the voltage output from the multimeter and output voltage reading were recorded in either 1 or 5 seconds intervals. The stock thermopile data was recorded in 1 [s] intervals for 180 [s] while Thermopile B had its output voltage read every 5 [s] for 300 [s].

3.5.1: Length of Thermopile Legs

The goal of this test was to see if the efficiency and power of the thermopile could be increased by reducing the length of the thermopile legs[18]. Output voltage in relation to the mass flow rate was compared between the stock thermopile with no combustion chamber and thermopile B with no combustion chamber. Thermopile B had the top of the thermocouples 15 [mm] from the top of the main tube.

3.5.2: Position of Thermopile B's Top Relative to the Top of the Main Tube

The distance between the top of Thermopile B and the top of the main tube (H) was altered to determine its effect on the overall performance of the thermopile. This absolute difference top of the thermopile and the top of the main tube was measured using digital calipers.[19]

[18] As described in 3.4.2

[19] Digital Calipers: Make – Mitutoyo Absolute Model: NTD 12-6" CX

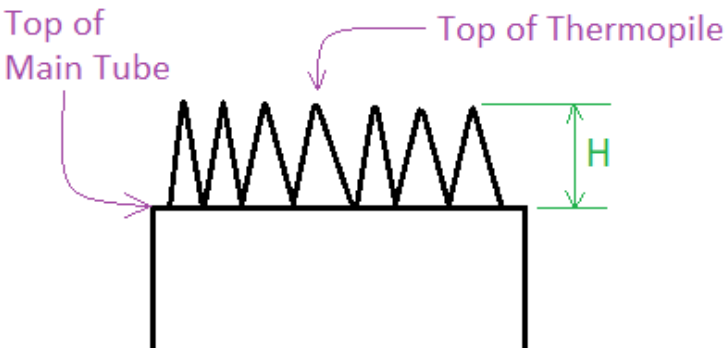

Figure 9: Nomenclature - Defining Variable H

3.5.4: Addition of a Combustion Chamber

The addition of combustion chambers and other features were explored. Four different combustion chamber designs were tested. The addition of a platinum wire to the combustion chamber design was done to help stabilize the flame in the chamber (Badra & Masri, 2012). Figure 10 shows the set up for Combustion Chamber 1 and Figure 11 shows the experimental set up for Combustion Chamber 2. Combustion Chamber 4 can be seen in Figure 12. The stock thermopile was used for all combustion chambers. The features of each combustion chamber design are shown in Table 2.

Table 2: Combustion Chamber Features

Combustion Chamber #	Features
1	Glass tube used as a combustion chamber
2	Glass disk used as a combustion chamber
3	Glass disk as combustion chamber with an aluminum foil reflective shield
4	Same as Combustion Chamber 3 but with a platinum wire along the top of the Glass Disk.

Figure 10: Combustion Chamber 1 Experimental Setup

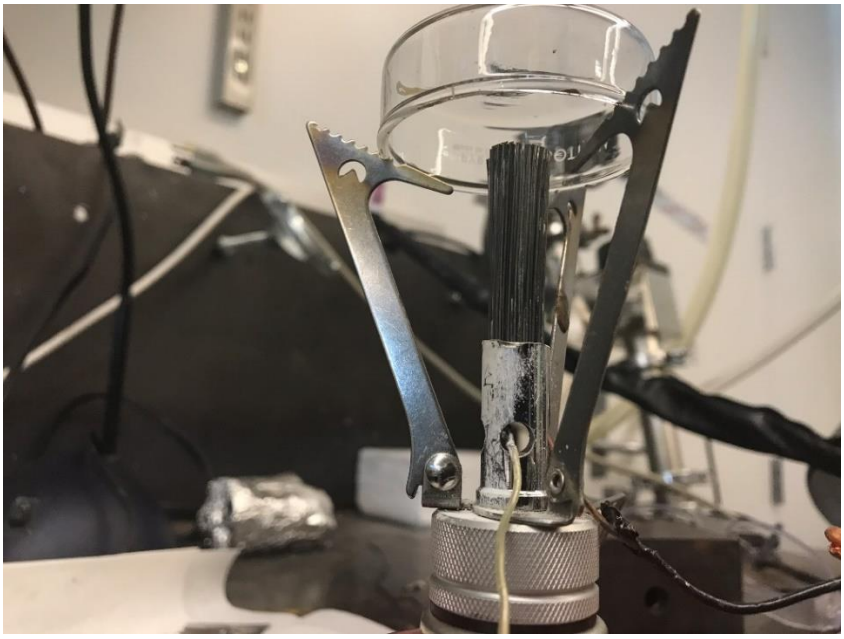

Figure 11: Combustion Chamber 2 Experimental Setup

Figure 12: Combustion Chamber 4

Chapter 4: Results

The data collected was organized so that the parameters that were altered on the TEG could be evaluated easily. To better compare the array of conditions tested, the output voltage was divided by the number of thermocouples in the respective thermopile and divided by the approximated mass flow rate. Dividing the output voltage by the number of thermocouples in the thermopile gives the average voltage produced by each thermocouple (V_{tcavg}). This helped to account for the difference in number of thermocouples each thermopile had. By additionally dividing V_{tcavg} by the approximated mass flow rate[20], the amount of fuel used to generate that voltage difference is accounted for. A higher input of fuel would result in a decrease of this value if temperature remains the same. This parameter is referred to as the Fuel Efficiency Coefficient (FEC or ζ) and has units of [V s/ kg], it was used to better isolate the effect of the parameter being analyzed and not the difference in fuel being supplied or the number of thermocouples the thermopile consists of. The equation for Fuel Efficiency Coefficient is shown below.

$$\zeta = \frac{V_{out}}{N_{tc}\,\dot{m}} \tag{4}$$

[20] Refer to Appendix E for derivation

Dimensions associated with the two different thermocouples can be found in Appendix C. All calculations were done with the help of Microsoft Excel.

4.1: Length of Thermopile Legs vs Performance

Two different thermopiles were examined for this test, the stock thermopile and Thermopile B. The primary focus of comparing the two thermopiles in similar conditions was to determine if the decrease in length would result in an increase in output. Reducing the length of the thermopile legs reduced the resistance in each leg and thus increased the overall output[21]. While decreasing the length of the thermopile leg could increase efficiency, the less length it had, the more the effects of conductive modes of heat transfer effected the achievable temperature differential between the two ends of the thermopile leg.

Figure 13 shows a plot of the Fuel Efficiency Coefficient of both the Stock Thermopile and Thermopile B vs time while Figure 14 shows the $V_{tc,avg}$ vs time for the two thermopiles. Table 3 shows a comparison of some performance parameters between the two TEG setups.

[21] Refer to 3.4.2: Thermopile B, for explanation

Table 3: Comparison between Stock Thermopile and Thermopile B, H=15 [mm]

Parameter	**Stock Thermopile**	**Thermopile B, H=15 [mm]**
Mass Flow Rate [kg/s]	1.43×10^{-4}	1.63×10^{-4}
Max Voltage Per Thermocouple [mV]	4.15	11.021

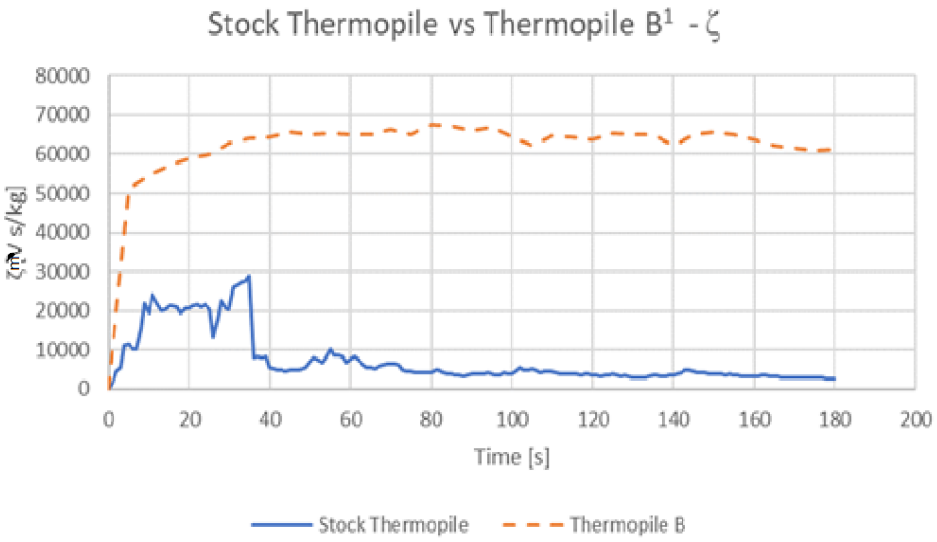

[1] Thermopile B with H=15 [mm]

Figure 13: Stock Thermopile vs Thermopile B[1] - ζ

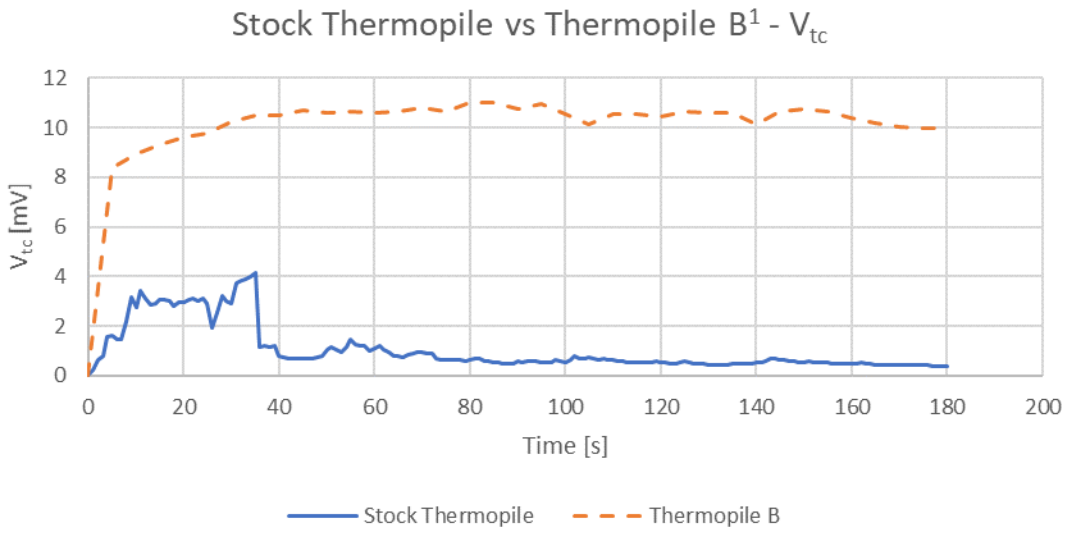

[1] Thermopile B with H=15 [mm]

Figure 14: Stock Thermopile vs Thermopile B[1] - V_{tc}

4.2 Position of Thermopile B's Top Relative to the Top of the Main Tube – Results

As discussed in 3.5.2, the distance between the top of thermopile B and the top of the main tube of the combustion device were varied between 0 and 15 [mm]. Table 4 states some of the performance parameters of the TEG for each H value tested. Figure 15 compares the FEC of various H values and Figure 16 compares the average voltage output per thermocouple vs time for those same H values. Lastly, Figure 17 shows the. relationship between the distance H and the max output voltage per thermocouple.

Table 4: Thermopile B Performance Parameters

ΔH [mm]	**Mass Flow Rate [kg/s]**	**Max Voltage Per Thermocouple [mV]**	**Average Voltage in SS zone[1] [mV]**	**Highest Voltage by Thermopile [mV]**
0	1.63×10^{-4}	2.815	2.620	22.525
1	1.70×10^{-4}	4.330	4.083	34.641
2	1.58×10^{-4}	2.948	2.780	23.587
3	1.75×10^{-4}	3.977	3.781	31.818
4	1.75×10^{-4}	6.251	5.763	50.006
5	1.85×10^{-4}	5.281	3.522	42.25
6	1.75×10^{-4}	4.133	3.377	33.068
8	1.82×10^{-4}	5.788	5.385	46.304
10	1.85×10^{-4}	12.068	9.712	96.546
12	1.63×10^{-4}	11.625	7.894	93.002
15	1.63×10^{-4}	11.021	10.366	88.168

[1]SS zone is after the voltage readings begin to level off and remain constant

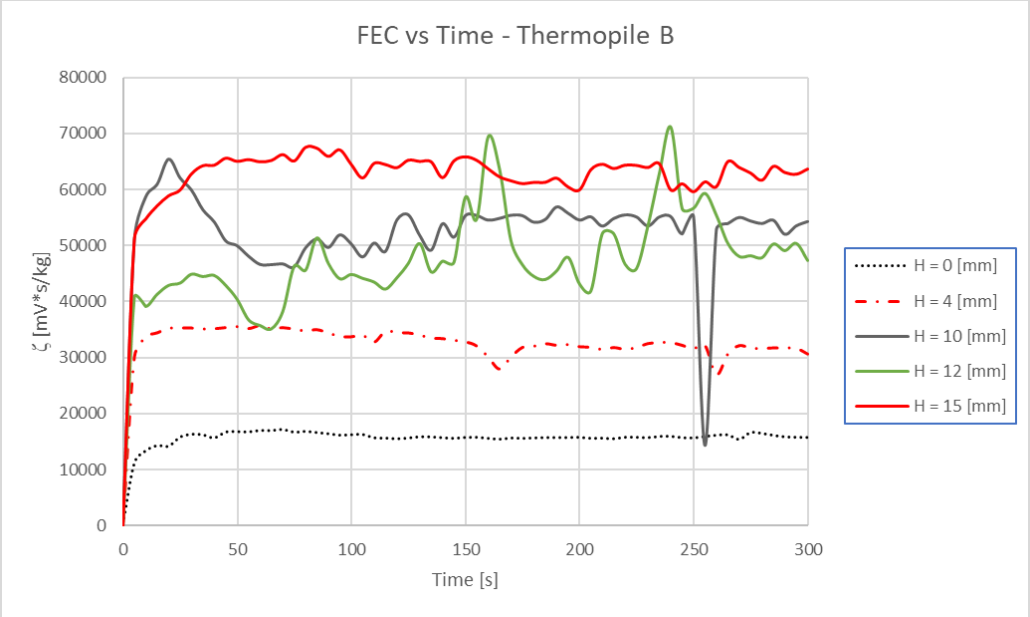

Figure 15: FEC vs Time – Thermopile B

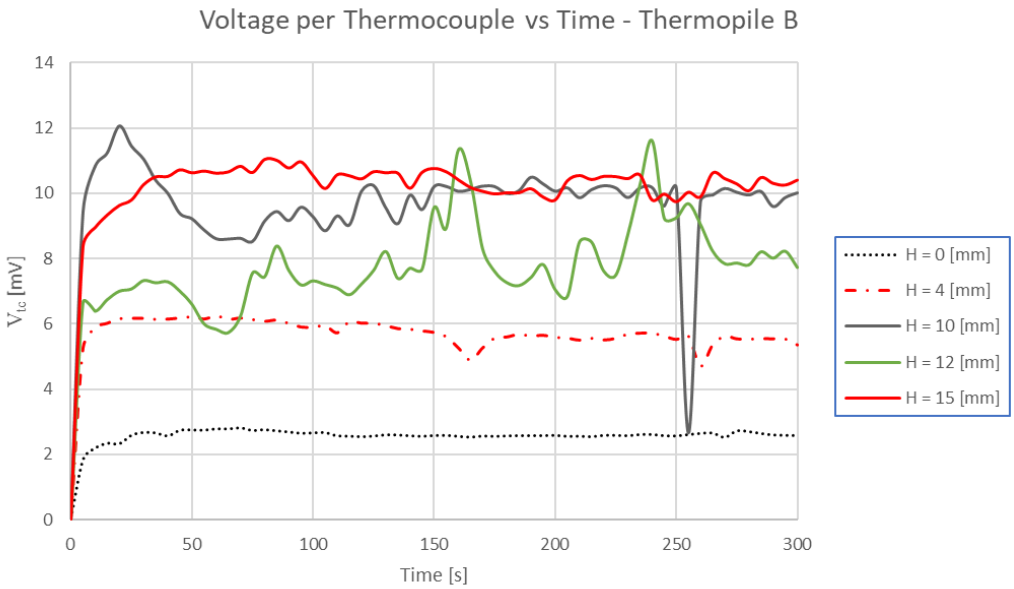

Figure 16: Thermopile B – Average Voltage per Thermocouple vs Time

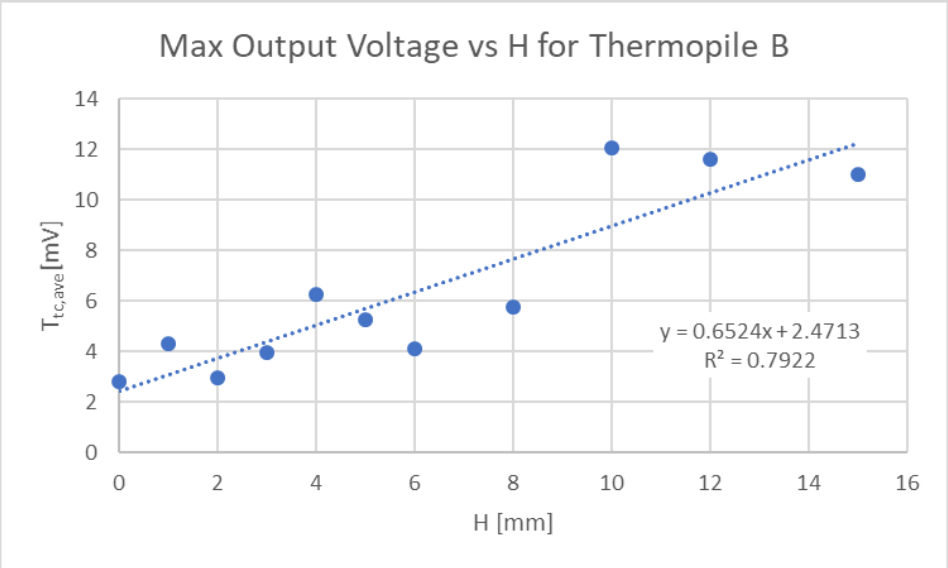

Figure 17: Thermopile B – Max Output Voltage vs H

4.3: Addition of Combustion Chamber Results

Four different shapes of combustion chamber designs were examined. An overview of the performance of each combustion chamber design is shown in Table 5. Figure 18 shows FEC vs time, Figure 19 illustrates average voltage per thermocouple. Table 6 shows the maximum and average power output [22] for each of the combustion chamber designs.

[22] Power output was determined by using the voltage outputs recorded and the resistance of the stock thermopile. Equation 5 shown below was used to determine the power output.

$$P = \frac{V^2}{R} \quad (5)$$

Table 5: Combustion Chamber Design Alteration Result Summary – 1

Combustion Chamber #	**Mass Flow Rate [kg/s]**	**Max Voltage Per Thermocouple [mV]**	**Average Voltage in SS zone[1] [mV]**	**Highest Voltage by Thermopile [mV]**
1	1.43 x 10-4	23.856	20.596	548.7
2	1.43 x 10-4	26.322	16.076	525.11
3	1.43 x 10-4	21.305	17.274	490.01
4	1.43 x 10-4	28.156	27.639	647.52

[1]SS zone is after the voltage readings begin to level off and remain constant

Table 6: Combustion Chamber Design Alteration Result Summary – 2

Combustion Chamber #	**Max Power Output [mW]**	**Average Power Output in SS zone[1] [mW]**
1	97.529	72.692
2	89.323	44.285
3	77.781	51.134
4	135.85	130.91

[1]SS zone is after the voltage readings begin to level off and remain constant

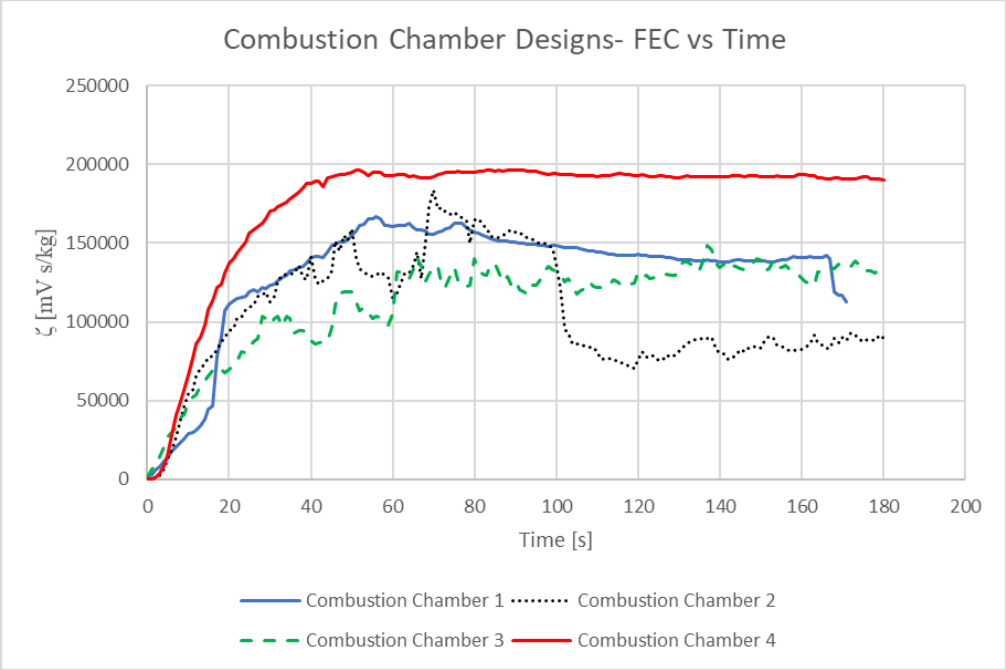

Figure 18: Combustion Chamber Designs – FEC vs Time

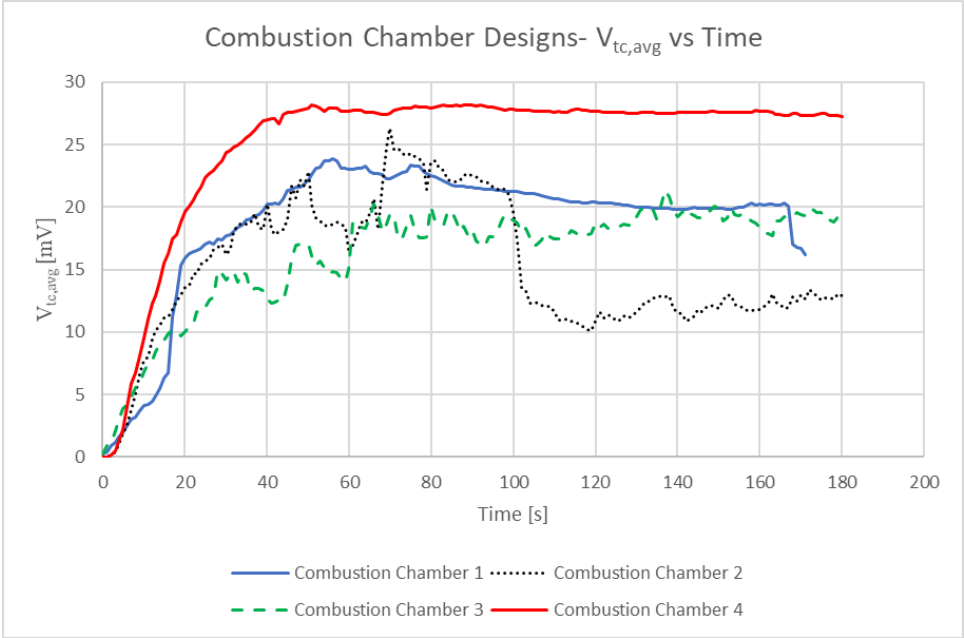

Figure 19: Combustion Chamber Designs – $V_{tc,avg}$ vs Time

4.4 Alteration of Mass Flow Rate of Combustion Chamber 4

When performing the experiments for different combustion chamber designs, it was noticed that Combustion Chamber 4 had the best overall performance. The mass flow rate was varied to see how the performance of the TEG changed. Figure 20 shows the FEC versus time of the three different mass flow rates while Figure 21 shows the average thermocouple voltage vs time for each case. Table 7 shows the mass flow rate, max power output of the TEG and the average power output after 30 seconds.

Table 7: Mass Flow Rates and Power Output of Combustion Chamber 4 Experiments

Combustion Chamber #	**Mass Flow Rate [kg/s]**	**Max Power Output [mW]**	**Average Power Output in SS zone[1] [mW]**
4a	1.43×10^{-4}	135.85	130.91
4b	1.31×10^{-4}	89.429	66.847
4c	1.65×10^{-4}	161.66	101.66

[1]SS zone is after the voltage readings begin to level off and remain constant

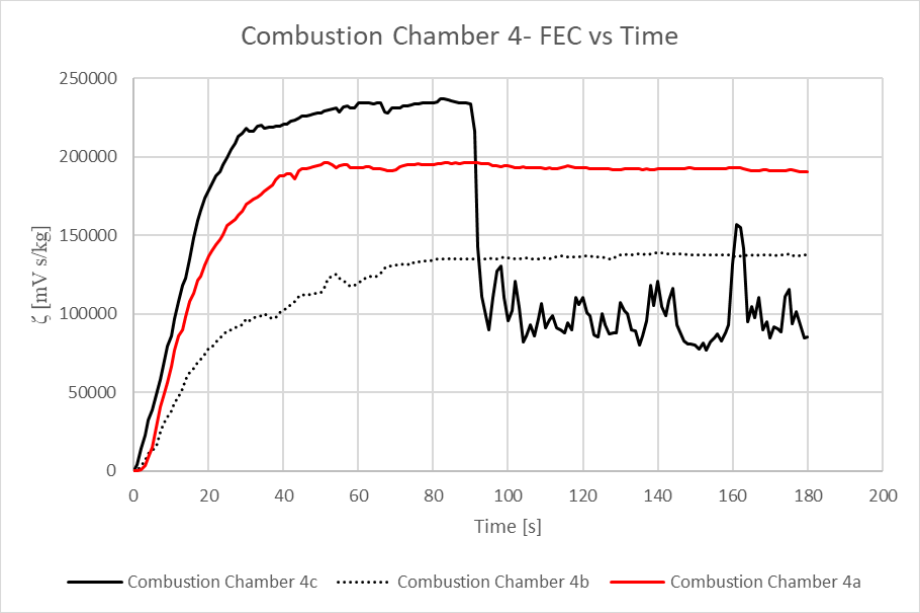

Figure 20: Combustion Chamber 4, Alteration of Mass Flow Rate – FEC vs Time

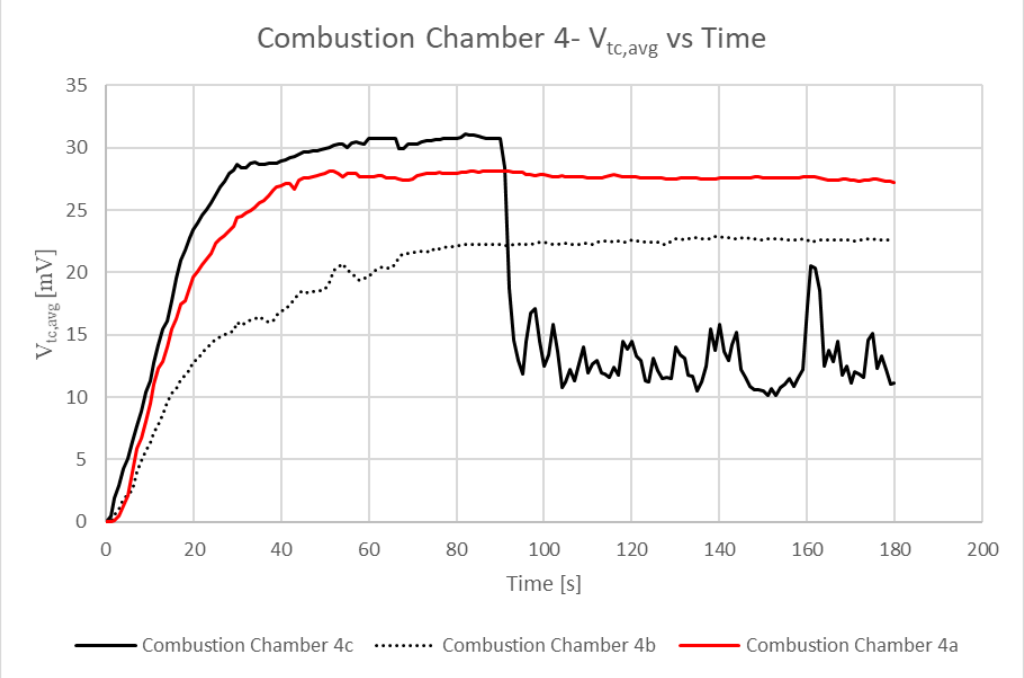

Figure 21:Combustion Chamber 4, Alteration of Mass Flow Rate – $V_{tc,avg}$ vs Time

4.5 Measure of Cold Side Temperature

Measuring the cold side temperature of thermopile was done using a Seek Thermal Compact Imager for an iPhone using spot mode. The flame and hot side temperature of the device were unable to be determined because it was beyond the capabilities of the camera.

While making temperature measurements of the TEG components, it was seen that the cold side of the thermopile and the base of the main tube remained at a consistent temperature of approximately 32 [^{o}C]. Figure 22 shows a picture of the thermal image used to determine the cold side temperature. Using the cold side temperature measured and the output voltage of the thermopile, the hot side temperature of the thermopile could be determined.

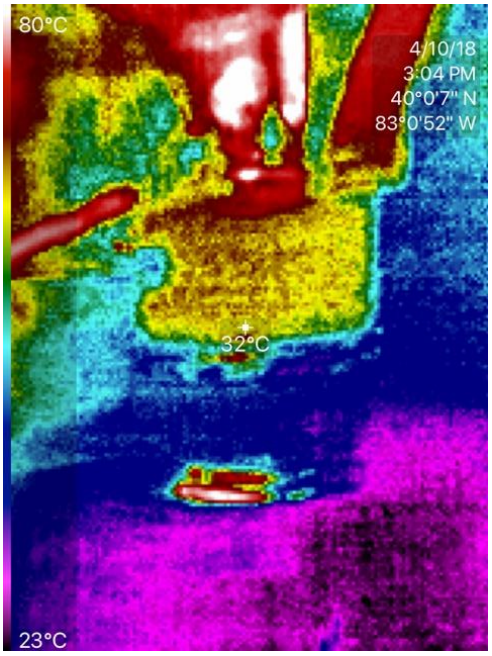

Figure 22: Cold Side Temperature Reading – Seek Thermal Compact Imager

Chapter 5: Discussion

Upon collection of the data and further examination, some trends associated with the alteration of the TEG design were noticed. Comparing both the FEC graphs to the average thermocouple output voltage, it is noticed that the shape of the graphs vary little. Therefore, it was concluded that the effects of the amount of fuel being used in the experiments did not have a substantial effect on the output voltage of the TEG since mass flow rates remained relatively the same across all experiments.

5.1 Length of Thermopile Legs– Discussion

When comparing the voltage output of Thermopile B to that of the stock thermopile, Thermopile B performs much better. The erratic behavior of the output voltage reading associated with the stock thermopile, however, are likely not the cause of leg geometry but rather the result of other factors.

When observing the data of the TEG for scenarios in which there is a combustion chamber, the voltage readings reach a steadier temperature reading. Data that was collected with the TEG without the use of a combustion chamber contained large output voltage fluctuations that are likely the result of erratic flame behavior and variations in heat transfer. Due to this behavior, the effect of the thermopile leg length could not be determined.

5.2 Position of Thermopile B's Top Relative to the Top of the Main Tube – Results

The position of the top of the thermocouple did influence the performance of the TEG. As the top of the thermopile moved away from the top of the main tube, the output voltage increased. When plotting the output voltage vs H, a clear relationship can be

seen[23]. A probable cause to this increase in output voltage as H increases is the tip of the thermopile being exposed to hotter temperatures. When the value of H is close to zero, the flame has not yet combusted at that location. This can be seen in Figure 23. Therefore, the output voltage was increasing due to an increase in temperature at the top of the thermopile.

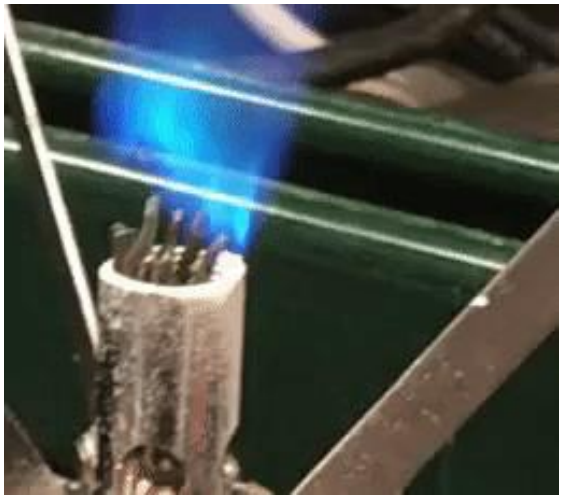

Figure 23: Thermopile B and Flame Behavior

An increase in the performance of the TEG will not continue as the value of H becomes larger. While the output voltage never trends downwards with the data collected, this is the cause of the thermopile being too short to continue to increase the value of H. Once the top of the thermopile is beyond the hottest point of the flame, the output voltage will begin to drop.

[23] Figure 17

5.3 Combustion Chamber Design

When comparing the results of the various combustion chamber designs, it was obvious that Combustion Chamber 4 performed the best. This combustion chamber obtained a high steady state voltage that remained consistent throughout the experiment. When comparing the performance of Combustion Chamber 3 and 4 and the difference in features between the two designs, it was concluded that the platinum had a considerable impact on performance.

While the addition of a combustion chamber is enough to boost the performance of the TEG, integrating a platinum wire helps to maintain a consistent output voltage. Therefore, it is believed that of all the parameters adjusted, the addition of a combustion chamber and a platinum wire had the most considerable impact.

5.4 Mass Flow Rate and TEG Performance

When adjusting the mass flow rate of the TEG with combustion chamber geometry 4, it was seen that decreasing the mass flow rate resulted in a decrease in output power. When the mass flow rate was increased, the output voltage increased. If the mass flow rate was increase too substantially, the entire thermopile can heat up and thus create a scenario where the entire thermopile is the same temperature and not creating electricity. This scenario occurred with Combustion Chamber 4c and can be seen in Figures 21 as the sharp decrease in average thermocouple output voltage around the 90 [s] mark. The entire thermopile leg heating up was likely the cause of an increase in flame temperature due to the combustion chamber retaining creating higher temperatures

and thus resulting in the entire leg heating up and decreasing the temperature differential of the leg and thus decreasing output voltage.

Chapter 6: Conclusion

Based on the examination of the data collected from this study, it was determined that the addition of a combustion chamber had the most significant impact on performance of the TEG. In addition to the major improvement seen with the addition of the combustion chamber, adding a platinum wire to the inside of the combustion chamber increased the output voltage delivered by the TEG.

A substantial increase in the performance of the TEG was seen when a combustion chamber was added due to less thermal losses between the flame and the thermopile. By decreasing these thermal losses, the temperature at the end of the thermopile increased, creating a larger temperature differential resulted in a larger output voltage.

Integration of the platinum wire ensured that complete combustion of the fuel occurred. Ensuring compete combustion, or close to it, kept the flame temperature steady and thus yielded more consistent output voltages.

6.1 Additional Applications

Determining the optimal geometry of a combustion chamber plays a significant role in the world outside of thermoelectric. Creating a combustion chamber that can easily attain a temperature close to the adiabatic flame temperature of a gas can greatly improve the efficiency of all heat engines, not just thermoelectrics.

This improvement in efficiency is due to the efficiency of heat engines being dictated by the difference in temperature between the hot and cool reservoir. The greater a temperature differential that can be created, the better the performance of the engine. Therefore, optimizing the geometry of a thermoelectric combustion chamber for fossil fuels has an important impact in understanding best practices to design an efficient heat engine.

6.2 Future Work

While it was determined that a platinum wire helps to stabilize the output voltage of the system, integrating platinum around the combustion chamber could result in a more efficient burn of the fuel and increase the temperature inside of the combustion chamber. The best option to decrease cost and improve performance would be to dip the top of thermopile. This is something that could be considered as a means of potentially improving the performance of the TEG.

In addition to implementing platinum around the combustion chamber, more thermocouples could be integrated into the design of the TEG. Thermocouples that run transverse to flow and/or ones heated by the exhaust gas of the combustion chamber could be investigate as a means of producing a higher output voltage for the same amount of fuel usage.

6.4 Summary

The geometry of a combustion chamber has a significant impact on the performance of a Thermoelectric Generator (TEG). While modern thermoelectric materials with high figures of merit exist, they often come at a cost that makes power production with

thermoelectrics cost prohibitive. Additionally, many thermoelectric materials that can withstand the temperatures associated with the flame temperature of combustible materials have poor figure of merits.

Since thermoelectrics are heat engines, however, their efficiency can be improved my increasing the temperature difference between the hot and cold side of the module. The larger a temperature differential that can be made with the use of an optimized combustion chamber geometry, the more efficient the TEG.

While improvements to the design of the combustion chamber were made, more improvements need to be made before a low cost and effective TEG can be created.

6.3 Contributions

In this study, the student was guided on the topic of study by both Joseph Heremans and Michael Adams. Both individuals helped guide the study in the right direction.

Bibliography

Accuratus. (2013). *Boron Nitride, BN Ceramic Properties*. Retrieved from Accuratus: https://www.amazon.com/MSR-11792-PocketRocket-Stove/dp/B000A8C5QE

Adiabatic Flame Temperature. (n.d.). Retrieved from http://web.mit.edu/16.unified/www/FALL/thermodynamics/notes/node111.html

Amazon. (n.d.). *MSR PocketRocket Stove*. Retrieved from Amazon.com: https://www.amazon.com/MSR-11792-PocketRocket-Stove/dp/B000A8C5QE

Badra, J. A., & Masri, A. R. (2012). Catalytic combustion of selected hydrocarbon fuels on platinum: Reactivity and hetero-homogeneous interactions. *Combustion and Flame*, 817-831.

Britannica. (1998, July 20). *Seebeck Effect.* Retrieved from Encyclopedia Britannica: https://www.brittannica.com/science/Seebeck-effect

Chen, Q., & Zheng, L.-R. (2011). Thermoelectric-Generator-Based DC-DC Conversion Network for Automotive Applications. *Journal of Electronic Materials*.

Chen, S., & Ren, Z. (2013, Oct. 10). Recent progress of half-Heusler for moderate temperature thermoelectric applications. *Materials Today*, pp. 387-395.

Corry, T. M., Moreland, W. C., & Strickland, E. L. (1960, June). Design of a 100-Watt Thermoelectric Generator. *Electrical Engineering*, pp. 482-488.

Design and Implementation of Thermoelectric Generator. (n.d.). Retrieved from Final Year Projects: http://myprojectscope.blogspot.com/2014/01/design-and-implementation-of.html

Engineering ToolBox. (2003). *Flame Temperatures Gases*. Retrieved from The Engineering ToolBox: https://www.engineeringtoolbox.com/flame-temperatures-gases-d_422.html

Engineering ToolBox. (n.d.). *Propane Butane Mixtures - Evaporation Pressures*. Retrieved from Engineering Toolbox: https://www.engineeringtoolbox.com/propane-butane-mix-d_1043.html

Katadyn Group. (2018). *Optimus*. Retrieved from Optimus Stoves: https://www.optimusstoves.com/us/us/235-8019961-optimus-gas-220-g-eu-en-fr-de-nl-it-es

Lasance, C. (2006, Nov. 1). *The Seebeck Coefficient*. Retrieved from Electronics Cooling: https://www.electronics-cooling.com/2006/11/the-seebeck-coefficient/

Liepmann, H. W., & Roshko, A. (1993). *Elements of Gasdyanmics.* New York: Dover.

MADA. (2018). *Laser Welding*. Retrieved from MADA: http://www.amadamiyachi.com/glossary/glosslaserwelding

MSR. (2018). *MSR ISOPRO*. Retrieved from MSR Gear: https://www.msrgear.com/msr-isopro-10

Plevyak, T. J. (1967, August). A 160-Watt Experimental Thermoelectric Power Plant for Telephone Microwave Equipment. *IEEE Trnasactions on Communication Technology*, pp. 571-578.

Rowe, D. (2006). *ThermoElectrics Handbook: Macro to Nano.* Baco Raton: CRC Press.

Sharma, S., Sheoran, G., & Shakher, C. (2012). Investigation of temperature and temperature profile in axi-symmetric flame of butane torch burner using digital holographic interferometry. *Optics and Lasers in Engineering*, 1436-1444.

Snyder, J. G. (2008, Fall). Small Thermoelectric Generators. *The Electrochemical Society*, pp. 54-56.

Thermocouple info. (n.d.). *Types of Thermocouple*. Retrieved from Thermocouple Info: https://www.thermocoupleinfo.com/thermocouple-types.htm

Wiegand, S. (2015, Feb.). Introduction to thermal gradient related effects, in Functional Soft Matter.

Zhang, X., & Zao, L.-D. (2015, January). Thermoelectric Materials: Energy conversion between heat and electricity. *Journal of Materiomics*, pp. 92-105.

Appendix A. Material Properties

Table 8: Fuel Material Properties (Engineering ToolBox, n.d.)

Mixture	Propane (C_3H_8) [%]	100	70	50	30	0
	Butane (C_4H_{10}) [%]	0	30	50	70	100
c_p [J/kg-K]		1630	1643.5	1652.5	1661.5	1675
R [J/kg-C]		188	174.5	165.5	156.5	143
γ		1.13	1.1198	1.113	1.1062	1.096

- Energy content of a pure propane mix: 95.8 [MJ/m^3] (Engineering ToolBox, n.d.)
- Energy content of a pure butane mix: 110.4 [MJ/m^3] (Engineering ToolBox, n.d.)

Table 9: Vapor Pressure of Propane/Butane Mixtures (Engineering ToolBox, n.d.)

Vapor Pressure [atm] (Absolute Pressure)						
Mixture	Propane (C3H8) [%]	100	70	50	30	0
	Butane (C4H10) [%]	0	30	50	70	100
		Pressure [atm]				
Temperature [C]	-42.2	-	-	-	-	-
	-34.4	1.46	-	-	-	-
	-28.9	1.78	1.32	-	-	-
	-23.3	2.19	1.61	1.24	-	-
	-17.8	2.67	2.03	1.51	1.16	-
	-12.2	3.32	2.39	1.84	1.40	-
	-6.7	3.86	2.90	2.21	1.69	-
	-1.1	4.61	3.49	2.67	2.05	-
	-4.4	5.43	4.13	3.21	2.46	1.21
	10.0	6.31	4.81	3.79	2.94	1.47
	15.6	7.34	5.63	4.40	3.49	1.78
	21.1	8.49	6.59	5.15	4.07	2.15
	26.7	9.71	7.53	6.04	4.68	2.57
	32.2	11.26	8.77	6.99	5.49	3.04
	37.8	13.04	10.13	8.09	6.38	3.59
	43.3	14.92	11.76	9.31	7.34	4.20

Table 10: Critical Pressures of Butane/Propane Mixtures[1]

P* [Pa] (Absolute Pressure)						
Mixture	Propane (C_3H_8) [%]	100	70	50	30	0
	Butane (C_4H_{10}) [%]	0	30	50	70	100
		Pressure [Pa]				
Temperature [C]	-42.2	5.35E+04	5.35E+04	5.35E+04	5.35E+04	5.35E+04
	-34.4	7.84E+04	5.35E+04	5.35E+04	5.35E+04	5.35E+04
	-28.9	9.53E+04	7.04E+04	5.35E+04	5.35E+04	5.35E+04
	-23.3	1.17E+05	8.63E+04	6.62E+04	5.35E+04	5.35E+04
	-17.8	1.43E+05	1.08E+05	8.10E+04	6.20E+04	5.35E+04
	-12.2	1.78E+05	1.28E+05	9.84E+04	7.52E+04	5.35E+04
	-6.7	2.07E+05	1.55E+05	1.19E+05	9.05E+04	5.35E+04
	-1.1	2.47E+05	1.87E+05	1.43E+05	1.10E+05	5.35E+04
	-4.4	2.91E+05	2.21E+05	1.72E+05	1.32E+05	6.46E+04
	10.0	3.38E+05	2.57E+05	2.03E+05	1.58E+05	7.89E+04
	15.6	3.93E+05	3.01E+05	2.36E+05	1.87E+05	9.53E+04
	21.1	4.55E+05	3.53E+05	2.76E+05	2.18E+05	1.15E+05
	26.7	5.20E+05	4.03E+05	3.23E+05	2.51E+05	1.38E+05
	32.2	6.03E+05	4.69E+05	3.74E+05	2.94E+05	1.63E+05
	37.8	6.98E+05	5.42E+05	4.33E+05	3.41E+05	1.92E+05
	43.3	7.98E+05	6.29E+05	4.98E+05	3.93E+05	2.25E+05

1 Red represents a mixture/temperature condition that does not choked flow through the jet.
Green represents a mixture/temperature condition that does a a choked flow condition through the jet.

Appendix B: Additional Figures

1. Figure 24 shows a picture of the early stages of the study. The Sterno fuel canister can be seen in Figure 24.

Figure 24: Combustion Device and Fuel Canister

2. Figure 25 shows the bag that the original thermopile, with its metal encasing, was delivered in. This metal encasing was later removed thus revealing the thermopile.

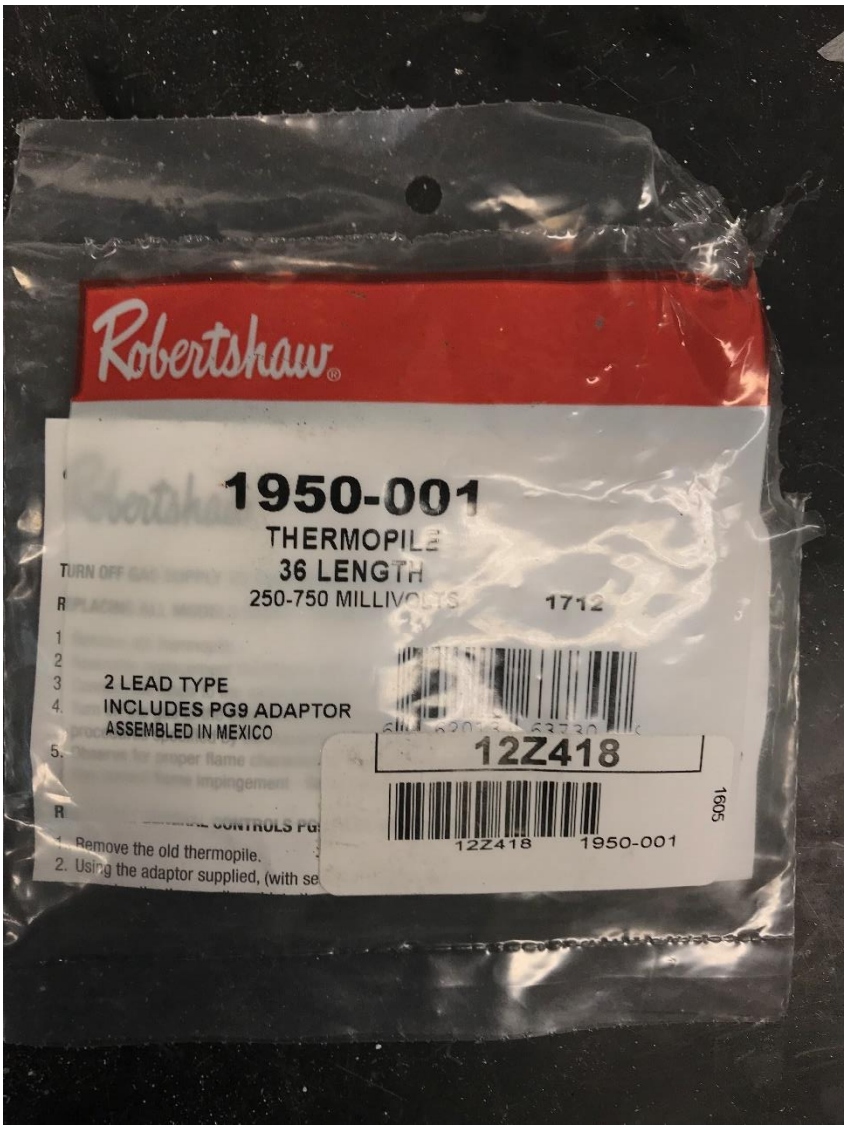

Figure 25: Thermopile Delivery Bag

3. Figure 26 shows the Dremel® tool with the reinforced cutoff wheel being used to cautiously grind down the metal encasing of the original thermopile.

Figure 26: Extracting Stock Thermopile from Original Thermopile Metal Encasing

4. Figure 27 shows the welder used to create thermopile B.

Figure 27: TIG Welder

Appendix C: Thermopile Details

Figure 28 shows the nomenclature used to describe the geometry of each thermocouple leg. All thermopile dimensions were done with the use of Dial Calipers[24] which had a resolution of 0.01 [mm].

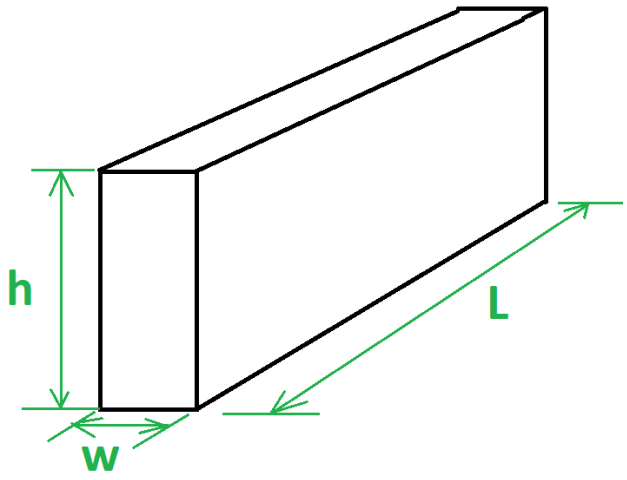

Figure 28: Thermopile Geometry Nomenclature

[24] Dial Calipers: Make – Mitutoyo Absolute Model: NTD12-6" CX

C.1: Stock Thermopile

Each leg of the stock thermopile had the same geometry, the values of the geometry are shown in Table 11. The junction points between each n-type and p-type materials appeared to have been joined through pressure welding.

The resistance of the stock thermopile was measured at 3.087 [ohms] in an isothermal condition.

Table 11: Stock Thermopile Dimensions

Number of Legs	46
L [mm]	49.00
h [mm]	1.18
w [mm]	0.30

C.2: Thermopile B

In thermopile B, each leg had a different length due to the way in which it was produced.[25] Table 11 gives the dimensions of the legs of thermopile B. Refer to Figure 29 as to which segments correlate to which leg.

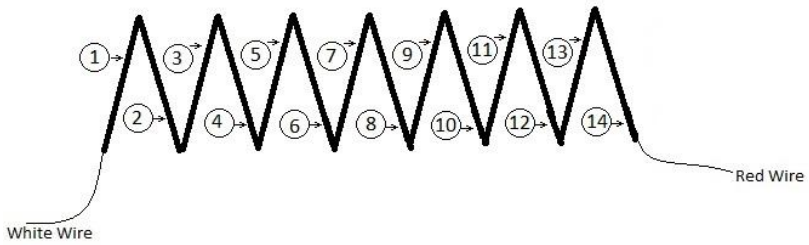

Figure 29: Thermopile B Segments

[25] Refer to Appendix D for a description on how thermopile B was produced.

Table 12: Thermopile B Dimensions

Thermopile B Dimensions			
Segment Number	**h [mm]**	**t [mm]**	**L [mm]**
1	1.25	0.40	13.38
2	1.25	0.40	20.07
3	1.25	0.40	19.73
4	1.25	0.40	19.84
5	1.25	0.40	19.81
6	1.25	0.40	18.82
7	1.25	0.40	16.82
8	1.25	0.40	16.80
9	1.25	0.40	16.94
10	1.25	0.40	20.06
11	1.25	0.40	19.98
12	1.25	0.40	19.70
13	1.25	0.40	16.11
14	1.25	0.40	18.67
15	1.25	0.40	19.16
16	1.25	0.40	10.43

Appendix D: Thermopile B Construction

During construction of thermopile B each material was marked with a color. Each color denoted the leg as either n-type or p-type and ensured that when the legs were joined back together, it would be in the correct orientation.

Once it was ensured that each leg was marked with the correct color, the center of each leg was marked and then cut with the use of a Dremel® tool with a reinforced cutool attachment. Upon successfully cutting the thermopile in half, the correct number of thermocouples were selected, placed in the correction orientation (n-type to p-type and vice versa), and then using Gas Tungsten Arc Welding (GTAW). Multiple methods of joining the two materials were attempted, these methods are described in the following sections of this Appendix. Figure 30 shows how the thermocouples were arranged before being welded using GTAW and Figure 31 shows the finished welds.

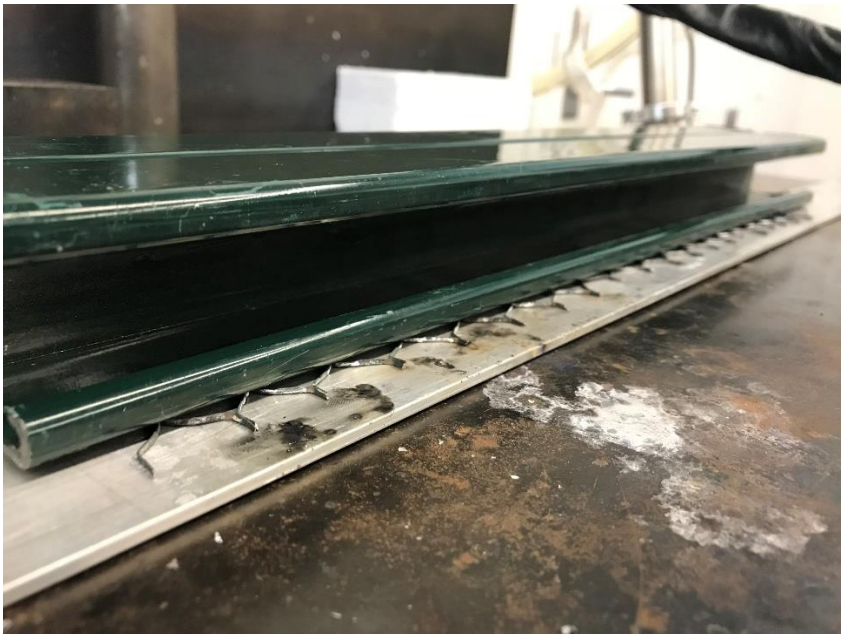

Figure 30: Pre-welding Setup

Figure 31: Post Gas Tungsten Arc Welding (GTAW)

D.1: Determining Weld Process

When first determining how to weld thermocouples in the lab, there was three approaches taken.

1. Spot Welding
2. Laser Welding
3. Gas Tungsten Arc Welding (GTAW)

The outcome of using each welding technique is described in their designed section.

D.1.1: Spot Welding

Spot welding was the first technique attempted. This technique was chosen first due to a spot welder already being set up in the lab to weld thermocouples used in other studies. Comparing the size of the wires welded to make thermocouples in other studies to the thermopile legs, there was a clear difference in size. The thermopile legs were significantly larger and would require a more power than what was being used to create the other thermocouples. After increasing the voltage on the spot welder and attempting to weld the thermocouple legs, there was no success in creating a strong weld and this method of welding was abandoned.

D.1.2: Laser Welding

The next method used to attempt to weld the thermopile legs together with was laser welding. Laser welding is a no contact process that uses an intense laser to rapidly heat the top side material which then bonds with the bottom material (MADA, 2018). For this welding process, it was required to take the materials to an outside location and have it performed there. The materials were taken to *All American Eye Glass Repair* on Bethal

Rd. in Columbus, Ohio. At this location, the two materials were bonded together using the laser welder at the store. Upon examination of the weld, it was of superior quality. When looking into the cost of having thermopile prototypes being welded at this location, it did not make economical sense. Due to cost constraints laser welding was no longer considered as a method to join thermopile legs.

D.1.3: Gas Tungsten Arc Welding (GTAW)

Gas Tungsten Arc Welding (GTAW), sometimes referred to as TIG welding, was the last method attempted to join the two thermopile legs together. A Thermal Arc Dragster 85 welder was used, a picture of the welder can be seen in Figure 26 in Appendix B. An arc was struck using a titanium rod on a steel plate and using the arc to use the two thermopile legs together.

Appendix E: Approximation of Mass Flow Rate of Fuel

When examining the data collected, determining the mass flow rate of the fuel was pertinent in making more accurate conclusion on the results. While the way the mass flow rate was not perfect, it gives approximate values to how various changes effected the performance of TEG.

E.1: Ideal Compressible Gas and Choked Flow

It was known that the fuel leaving the canister would be at the vapor pressure of the of the gas at approximately the same temperature as the room. Additionally, the fuel leaving the canister was treated as an ideal compressive fluid[26] in 1 dimensional flow. Therefore using equation (6), the critical pressure was determined for various propane/butane mixtures. This table can be seen in Appendix A in Table 9.

$$\frac{P^*}{P_0} = 0.5283 \tag{6}$$

When examining the data collected by the student, all conditions when data was collected occurred when choked flow conditions were met. Therefore, using the relationships used for choked flow conditions (Liepmann & Roshko, 1993) and utilizing the flow function, equation 5, the mass flow rate was determined based on the area of the jet opening.

[26] Definition of an ideal fluid is given in (Liepmann & Roshko, 1993)

$$F = \frac{\gamma}{\sqrt{\gamma - 1}}\left[1 + \frac{\gamma - 1}{2}\right]^{-\left(\frac{(\gamma+1)}{2(\gamma-1)}\right)} \tag{7}$$

$$F = \frac{\dot{m}\sqrt{c_p T_{room}}}{A_{jet}\, P_0} \tag{8}$$

By solving for F using equation 5 and solving for $\dot{m}$ using equation 6, the approximate mass flow rate of the system was determined based on the amount of jet area open due to the fuel valve. The amount of area open was approximated using geometric relations and the assumption that the object covering the hole is straight, such as Figure 32 demonstrates.

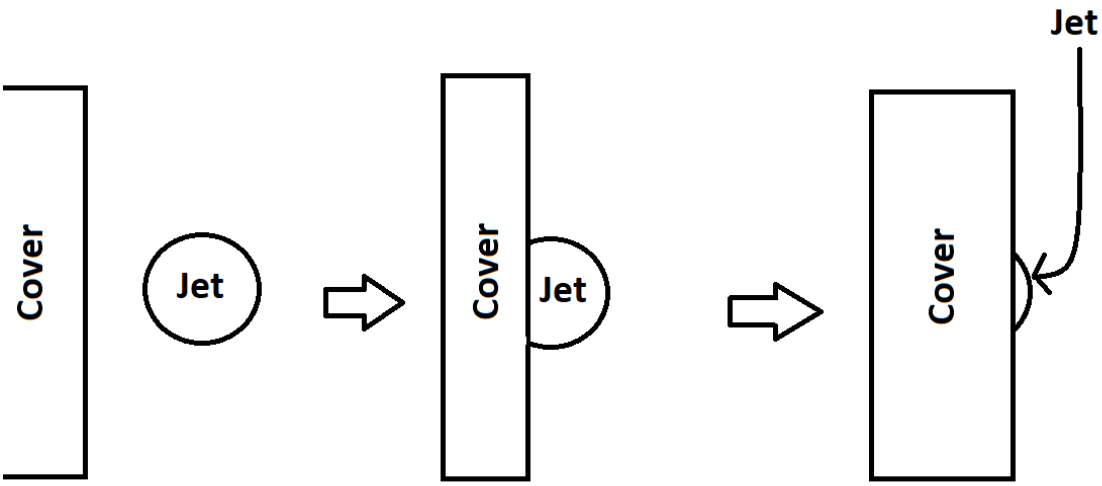

Figure 32: Jet Area Approximation

Through research online, it was determined that the approximate Jet diameter of the PocketRocket® is 0.3 [mm]. A correlation between the amount the fuel valve is rotated and the position of the cover[27]. Using this correlation, the amount area exposed to flow was then used to approximate the mas flow rate of the fuel using equation 7 (Liepmann & Roshko, 1993).

$$\dot{m} = \frac{F A_{jet} P_0}{\sqrt{c_p T_{room}}} \tag{9}$$

Mass flow rates between ranged between 1.85×10^{-4} and 1.43×10^{-4} [kg/s]. Mass flow rate was assumed to remain constant so long as the fuel valve is not tampered with.

[27] It took 1.5 rotations of the fuel valve to completely cover the jet.